AGU PUBLICATIONS

JGR

Journal of Geophysical Research: Space Physics

RESEARCH ARTICLE
10.1002/2014JA020518

Key Points:
- Hiss intensities are high during high-solar wind pressure (HSWP) intervals
- During HSWP intervals and $L > 7$, hiss is coherent or quasi-coherent
- On average hiss intensities are larger on the dayside than on the nightside

Correspondence to:
B. T. Tsurutani,
bruce.t.tsurutani@jpl.nasa.gov

Citation:
Tsurutani, B. T., B. J. Falkowski, J. S. Pickett, O. Santolik, and G. S. Lakhina (2015), Plasmaspheric hiss properties: Observations from Polar, *J. Geophys. Res. Space Physics*, *120*, doi:10.1002/2014JA020518.

Received 19 AUG 2014
Accepted 17 DEC 2014
Accepted article online 19 DEC 2014

Plasmaspheric hiss properties: Observations from Polar

Bruce T. Tsurutani[1], Barbara J. Falkowski[1,2], Jolene S. Pickett[3], Ondrej Santolik[4,5], and Gurbax S. Lakhina[6]

[1]Jet Propulsion Laboratory, California Institute of Technology, Pasadena, California, USA, [2]Glendale Community City College, Glendale, California, USA, [3]University of Iowa, Iowa City, Iowa, USA, [4]Institute of Atmospheric Physics, Czech Academy of Sciences, Prague, Czech Republic, [5]Faculty of Mathematics and Physics, Charles University, Prague, Czech Republic, [6]Indian Institute of Geomagnetism, Navi Mumbai, India

Abstract In the region between $L = 2$ to 7 at all Magnetic Local Time (MLTs) plasmaspheric hiss was detected 32% of the time. In the limited region of $L = 3$ to 6 and 15 to 21 MLT (dusk sector), the wave percentage detection was the highest (51%). The latter plasmaspheric hiss is most likely due to energetic ~10–100 keV electrons drifting into the dusk plasmaspheric bulge region. On average, plasmaspheric hiss intensities are an order of magnitude larger on the dayside than on the nightside. Plasmaspheric hiss intensities are considerably more intense and coherent during high-solar wind ram pressure intervals. A hypothesis for this is generation of dayside chorus by adiabatic compression of preexisting 10–100 keV outer magnetospheric electrons in minimum B pockets plus chorus propagation into the plasmasphere. In large solar wind pressure events, it is hypothesized that plasmaspheric hiss can also be generated inside the plasmasphere. These new generation mechanism possibilities are in addition to the well-established mechanism of plasmaspheric hiss generation during substorms and storms. Plasmaspheric hiss under ordinary conditions is of low coherency, with small pockets of several cycles of coherent waves. During high-solar wind ram pressure intervals (positive *SYM-H* intervals), plasmaspheric hiss and large L hiss can have higher intensities and be coherent. Plasmaspheric hiss in these cases is typically found to be propagating obliquely to the ambient magnetic field with θ_{kB0} ~30° to 40°. Hiss detected at large L has large amplitudes (~0.2 nT) and propagates obliquely to the ambient magnetic field (θ_{kB0} ~70°) with 2:1 ellipticity ratios. A series of schematics for plasmaspheric hiss generation is presented.

1. Introduction

Plasmaspheric hiss is a "structureless," low-frequency electromagnetic whistler-mode emission detected within the plasmasphere. When it is played through a loudspeaker, it has a hiss-like sound, thus the name [*Thorne et al.*, 1973]. Since the original discovery of these waves in the magnetosphere by *Russell et al.* [1969] and *Dunckel and Helliwell* [1969], there have been numerous studies concerning the wave properties [*Thorne et al.*, 1974; *Solomon et al.*, 1988; *Gail et al.*, 1989; *Gail and Inan*, 1990; *Storey et al.*, 1991; *Hayakawa and Sazhin*, 1992; *Cornilleau-Wehrlin et al.*, 1978, 1993; *Santolik et al.*, 2001; *Shinbori et al.*, 2003; *Meredith et al.*, 2004, 2006; *Green et al.*, 2005; *Tsurutani et al.*, 2012; *Summers et al.*, 2014].

Hiss-like waves have also been detected in detached high density plasma regions outside of the nominal plasmaspheric region, particularly in the dusk-evening side region [*Chan and Holzer*, 1976; *Cornilleau-Wehrlin et al.*, 1978; *Parrot and Lefeuvre*, 1986]. These waves have characteristics that are similar to plasmaspheric hiss and are believed to be the same emission. We will call the latter waves "hiss" to distinguish them from hiss detected within the plasmasphere proper.

Plasmaspheric hiss is known to occur during geomagnetic quiet intervals [*Russell et al.*, 1969; *Dunckel and Helliwell*, 1969]. It is also detected at intensified levels during substorms [*Thorne et al.*, 1973, 1974, 1977; *Hayakawa et al.*, 1986; *Meredith et al.*, 2004; *Li et al.*, 2013] and magnetic storms [*Smith et al.*, 1974; *Tsurutani et al.*, 1975; *Delport et al.*, 2012; *Golden et al.*, 2012]. *Thorne et al.* [1979] proposed the generation of quiet time plasmaspheric hiss as due to recycling of trapped waves through an equatorial amplification region just inside the plasmapause. *Chum and Santolik* [2005] and *Santolik et al.* [2006] showed that earthward propagating chorus could be considered as a possible candidate for the source of plasmaspheric hiss. These results were confirmed and expanded upon by *Bortnik et al.* [2008, 2009a, 2009b]. The latter authors argued that during geomagnetic active times, outer zone chorus penetrates into the plasmasphere at low altitudes and becomes

plasmaspheric hiss. Ray tracing studies by *Chen et al.* [2012] and wave propagation observations by *Wang et al.* [2011] and *Tsurutani et al.* [2012] have shown general agreement with the Bortnik et al. model. However one should be cautious in this assessment. Please see arguments in *Santolik and Chum* [2009].

Meredith et al. [2006] have attempted to identify how much hiss within the plasmasphere is naturally generated by either energetic (~10 to 100 keV) electron instabilities or by lightning-generated whistlers [*Dragonov et al.*, 1992]. *Meredith et al.* [2006] concluded that the wave power above ~2 kHz is more related to lightning-generated whistlers, whereas lower frequency emissions are generated by plasma instabilities. *Li et al.* [2013] have found that hiss is generated locally inside the plasmasphere by substorm electrons in the outer portion of the plasmasphere. The naturally generated emissions can have frequencies as low as ~20 Hz. *Chen et al.* [2014] have shown that generation of such unusually low-frequency plasmaspheric hiss can be explained by the recycling of waves through the equatorial amplification region as proposed by *Thorne et al.* [1979].

It is the purpose of this present effort to study plasmaspheric hiss using 1 year of Polar spacecraft data. The frequency range of the waves studied will be limited to ~22 Hz to 2 kHz, focusing this study on naturally generated waves (by instabilities). Magnetosonic waves have been removed from the data set. We also remove chorus waves which are identified by their bursty, elemental (~0.2 s) structures. We perform statistical studies to determine the L-MLT location and intensity of the emissions, the geomagnetic activity (*AE* and *SYM-H*) dependences, and the wave occurrence frequency and intensities as functions of magnetic latitude (MLAT). The purpose of this study is to provide a database for future wave-particle modeling. Detailed case studies will be performed to determine differences in wave properties as a function of MLAT (equatorial and high latitude), and those in extended *L* regions (presumably within plasma tails) from those within the plasmasphere proper. Wave coherency analyses will be performed on the above cases as well. From these results, comments will be made about applications for wave-particle interaction modeling and also about plasmaspheric hiss origins. A somewhat new perspective for both will be proposed in section 5 of the paper.

2. Method of Data Analyses

One year of Polar Plasma Wave Instrument (PWI) data [*Gurnett et al.*, 1995] has been analyzed to study plasmaspheric hiss: 1 April 1996 to 4 April 1997. Only waves at and inside the plasmapause were included. The plasmapause was identified by the in situ electron plasma frequency characteristics in the wave data plots [*Santolik et al.*, 2001]. As previously mentioned, magnetosonic and chorus waves were removed from the data set. This was done by hand inspection [see *Tsurutani et al.*, 2014a].

Because there were instrumental problems with the electric field *E* measurements within the high density plasmasphere (at times, there were preamplifier oscillations which corrupted the measurements), the wave surveys that follow will be conducted for only the magnetic field component (*B*) of the waves. For the statistical surveys, the ~2 kHz bandwidth High-Frequency Waveform Receiver (HFWR) data covering the frequency range ~20 Hz to 2000 Hz, obtaining ~0.5 s snapshots every ~2 min interval [*Santolik et al.*, 2001], were used. The ~2 min interval is used as a basis for our statistical studies and will hereby be called an "interval" or "background." If plasmaspheric hiss was detected during the interval, it will be called a "wave event."

It should be noted that plasmaspheric hiss often was continuous detected for tens of minutes. All of those data were used. These data are not statistically independent. In fact no spacecraft wave survey done in the past was statistically significant, nor have the authors claimed that they were.

There were 1013 Polar inbound and 1013 outbound crossings, or a total of 2026 passes during the year of the study. Of these, there were 814 passes where the Polar HFWR wave data overview plots were available. For each pass, there are many 2 min intervals and thereby many possible wave events. As previously mentioned, these latter 814 passes with many ~2 min intervals are the basis for the statistical part of this study. We call these possible intervals of waves our background for our study.

The ~2 min plasmaspheric hiss events were examined in detail for specific cases. For these studies, the high time resolution ~0.5 s plasma wave data (PWI 2 kHz HFWR data) [*Gurnett et al.*, 1995] were analyzed. A minimum variance method [*Smith and Tsurutani*, 1976] was used to identify the wave direction of propagation, *k* [*Verkhoglyadova et al.*, 2010], and the wave polarization. The maximum variance field

component (B1) and intermediate variance field component (B2) obtained from the output of the minimum variance analyses were cross correlated to identify the level of wave coherency. See *Tsurutani et al*. [2009, 2011a] for examples of prior results from this method.

The wave "noise" is not well known in the plasmasphere. To our knowledge, no one has tried to identify this phenomenon. It also may be time varying. Thus, when minimum variance analyses were performed on several cycles of the waves in our analyses, the wave intervals were typically selected because they indicated one wave was clearly present. In the minimum variance analyses, λ_1, λ_2, and λ_3 correspond to the maximum, intermediate, and minimum eigenvalues, respectively. The ratio λ_2/λ_3 which gives the accuracy or "error" in the determination will be given in each case. A value of >10 for the ratio indicates that the wave was well determined. The typical case where it was found that the waves were incoherent, it is suspected that there may be many waves propagating in different directions causing the incoherence. A technique has been developed for identifying two separate wave packets [*Storey and Lefeuvre*, 1979; *Lefeuvre et al*., 1981; *Buchalet and Lefeuvre*, 1981; *Goldstein and Tsurutani*, 1984] but not one for many wave packets. This topic is beyond the scope of the present paper and thus will not be addressed here.

The λ_1/λ_2 ratio gives the degree of wave polarization (however, see caveats in *Tsurutani et al*. [2011a]). A ratio of 1.0 corresponds to circular polarization and higher values to elliptical polarization.

Magnetosonic (MS) waves were also detected inside the plasmasphere [*Tsurutani et al*., 2014a]. This mode of electromagnetic (EM) waves is linearly polarized and has magnetic perturbations aligned with the ambient magnetic field, B_0. The direction of $\mathbf{B_0}$ is obtained from the magnetometer instrument on board Polar. Plasmaspheric hiss is a transverse EM mode with magnetic perturbations orthogonal to $\mathbf{B_0}$ (when k is parallel to $\mathbf{B_0}$), so the two modes are easily distinguished from each other. In all of the MS wave cases near the magnetic equator, the MS wave intensities were higher than those of the hiss. These MS events were removed from the data set and are not used in the statistical survey portion of our study. Chorus elements have sharp frequency-time structures of ~0.2 s duration [*Tsurutani et al*., 2013]. These emissions were easily identified in the data set and were removed when identified.

The time period of data analyses was solar minimum. This is a general time period with a lack of intense magnetic storms [*Tsurutani et al*., 2006, 2011b]. The geomagnetic activities expected are High-Intensity Long-Duration Continuous *AE* Activity (HILDCAA) events [*Tsurutani and Gonzalez*, 1987; *Hajra et al*., 2013] with somewhat weaker solar wind streams and HILDCAA intensities than during the solar declining phase [*Tsurutani et al*., 2011b].

The solar wind data were obtained from the OMNI website at http://omniweb.gsfc.nasa.gov/. The interplanetary data had already been time adjusted to take into account the solar wind convection time from the spacecraft to the magnetosphere. The *AE* and *SYM-H* data used in this study were obtained from the World Data Center for Geomagnetism at Kyoto University.

In the section 3 of the paper, we attempt to determine the dependence of plasmaspheric hiss on geomagnetic activity, specifically for the *AE* and *SYM-H* indices. The question is how can one do this properly? This is a difficult problem. What kind of time lags should one take? Almost all plasmaspheric hiss generation mechanisms proposed in the literature assume that the waves are generated by energetic ~10–100 keV anisotropic electrons. For the portion of plasmaspheric hiss that is generated during substorms and storms by direct midnight sector injection [*Thorne et al*., 1973, 1974, 1977; *Smith et al*., 1974] this time delay with *AE* and *SYM-H* should be small or zero. The gradient and curvature drift speed of electrons to the dayside will be tens of minutes (depending on the energy) and to the duskside region, still larger. This is simple if the electrons drift to the duskside plasmaspheric bulge and then enter the plasmasphere there. However, if the bulge extends with time to go to the L shell of the drifting electrons, these delay times will be hours or even days. Another possible hiss generation mechanism is outer zone chorus which is generated in the outer magnetosphere and then propagates into the plasmasphere. Using the drift time for the energetic electrons to drift to the spacecraft local time presumes that the hiss was first generated as chorus and the waves propagate along constant MLT zones inward to become plasmaspheric hiss. But this does not address the possibility of the chorus propagation to other MLT zones.

We wish to avoid making presumptions prior to doing the statistical surveys. Thus, for the initial part of the survey, we will assume no time delays whatsoever. After we obtain some initial results, we will attempt to analyze the data with specific time delays. This will be discussed in the body of the text in the appropriate sections.

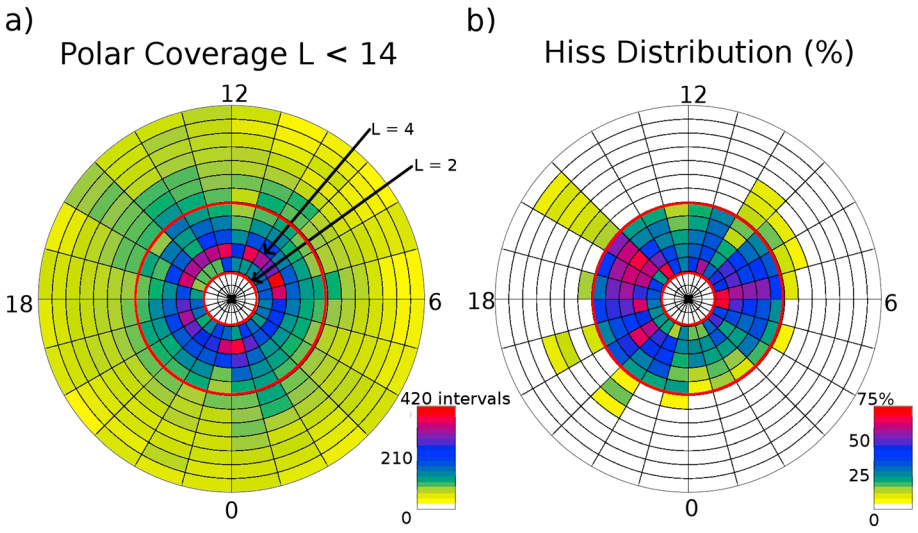

Figure 1. (a) The distribution in *L* and MLT of the spacecraft coverage over the year. Noon is at the top and dawn is on the right. The *L* coverage extends from 2 (the outer edge of the white area at the center) to 14, radially outward. The legend gives the number of ~2 min intervals for each ΔL-ΔMLT bin. (b) The percent occurrence of plasmaspheric hiss events for each ΔL-ΔMLT bin. Red rings are shown at $L = 2$ and $L = 7$ in both panels for general guidance to the *L* values.

3. Results

3.1. Hiss Location

Figure 1 shows the magnetospheric coverage for the study. Figure 1a gives the L-MLT distribution of coverage. The legend at the bottom right gives the number of ~2 min passes in each of the $\Delta L = 1$ and $\Delta\text{MLT} = 1$ h bins. The coverage in space from $L = 2$ to 14 and all MLT is quite good. For reference, we call this the background distribution. Figure 1b shows the distribution of plasmaspheric hiss in percent occurrence. This is the number of wave events divided by the background for each bin. The legend is given in the lower right-hand side. Several interesting features can be noted in this distribution. First, plasmaspheric hiss can be detected at $L = 2$ to 7 (red rings for both panels) and all MLTs. Plasmaspheric hiss has a strong tendency for its greatest occurrence (up to 75%) for $L = 3$ to 6 and MLT from 15 to 21 (dusk sector). There is also a small region of enhancement near MLT ~0600. The regions of minimum occurrence frequency are near noon and midnight.

There are some intervals where the waves extend to relatively large *L* values (~10). These intervals are mostly on the dusk-evening side. Since these events may be occurring in "plasma tails," "plumes," [*Grebowsky*, 1970] or "plasmaspheric bulges" [*Chappell*, 1974], these events will be referred to simply as hiss to distinguish these emissions.

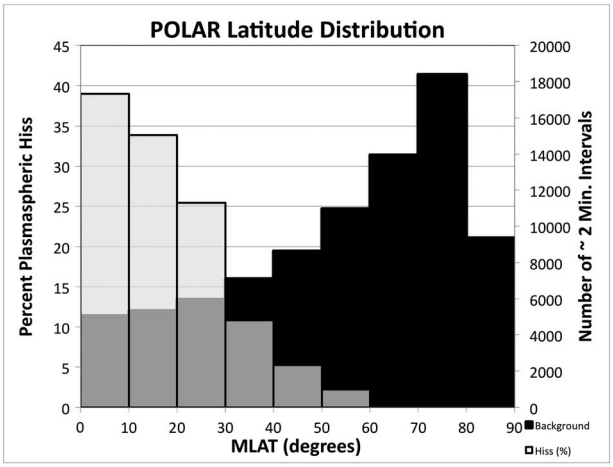

Figure 2. The latitude distribution of plasmaspheric hiss (grey/white bars).

To determine the general distribution of plasmaspheric hiss, the averages of the bin percentages shown graphically in Figure 1 were calculated. It is found that from $L = 2$ to 7, for all local times, the average was 32%. If one limits the magnetic local time to 15 to 21 MLT, the average is higher, 42%. If one further limits *L* to the range from 3 to 6 (for the same MLT range), the percent occurrence rate is 51% (with peak intensities up to 75%, shown in Figure 1).

The plasmaspheric hiss magnetic latitude distribution is shown in Figure 2. Two histograms are shown in this figure, the background (spacecraft coverage)

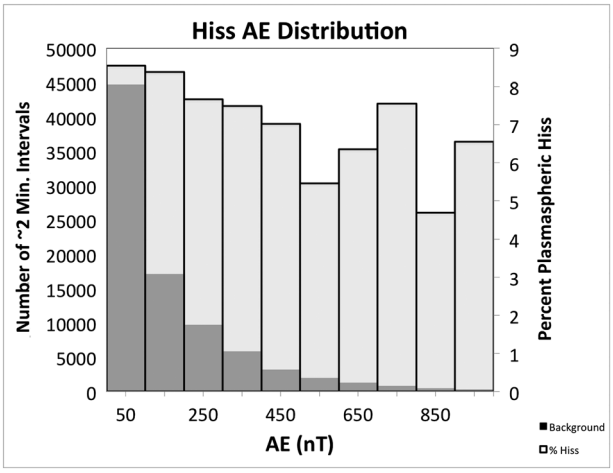

Figure 3. The plasmaspheric hiss dependence on geomagnetic activity (*AE*). The format is similar to that in Figure 2. There are no time delays assumed between *AE* and the waves here. Plasmaspheric hiss percent occurrence is shown in light grey and the background in dark grey.

distribution is given in black and the percent plasmaspheric hiss occurrence rate in grey/white. The background is the same 2 min events as in Figure 1. The background is plotted behind the percent occurrence of plasmaspheric hiss, so where the two plots overlap, the background appears as dark grey. The scale for the background "number of intervals" is on the right *y* axis, and the scale for the percent plasmaspheric hiss occurrence is on the left *y* axis.

The percent occurrence of plasmaspheric hiss is greatest at the equator, 38%. This value decreases to ~25% at 20°–30° latitude and then falls off quite rapidly at higher latitudes. There was no plasmaspheric hiss detected at MLAT values above 60° due to Polar orbital constraints. The spacecraft was not within the plasmasphere at MLAT $>$ 60°.

3.2. Hiss Geomagnetic Activity Dependence

One of the fundamental questions concerning the property of all magnetospheric plasma waves is "do the waves occur during enhanced geomagnetic activity?" We address the *AE* (substorm) dependence of plasmaspheric hiss in Figure 3 and the *SYM-H* dependence of plasmaspheric hiss in Figure 4.

Figure 3 shows the plasmaspheric hiss dependence on the *AE* index in light grey. The scale is on the right. As previously mentioned, no time delay was taken into consideration in assigning the *AE* value for a particular interval. This is what one would assume if all of the plasmaspheric hiss were generated by plasma sheet injection of ~10–100 keV electrons into the nightside sector of the plasmasphere. The background number of events is shown in dark grey, with the scale on the left-hand *y* axis. The main feature that can be noted in the figure is that plasmaspheric hiss occurs at all values of *AE*. The percent occurrence is between 4.7% at *AE* = 0 nT and 8.6% at *AE* = 800 nT. Actually, plasmaspheric hiss has slightly higher percent occurrence rates for the lowest *AE* range (~0 to 500 nT).

To address one referee's question, we examined the plasmaspheric hiss using the *AE* values 30 min and 1 h prior to the hiss detection. The same general *AE* distributions were obtained. Since these provided no new interesting information, they have not been shown to save space.

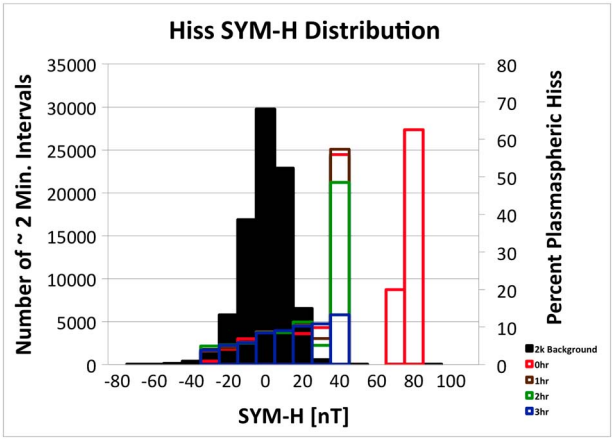

Figure 4. Plasmaspheric hiss dependence on the *SYM-H* index. The format is similar to those in Figures 2 and 3. The *SYM-H* indexes 0 h (red), 1 h (brown), 2 h (green), and 3 h (blue) before the wave event are also shown.

Figure 3 also shows that most of the plasmaspheric hiss detected in this survey occurred when *AE* was less than 250 nT or outside of substorms. This is because the most of the intervals (see the background) occurred during these low-*AE* values.

Figure 4 shows the plasmaspheric hiss dependence on the magnetic storm index, *SYM-H*. The *SYM-H* background is given in solid black, with the legend of number of events shown as the *y* axis on the left. The percent occurrence of plasmaspheric hiss with no delay time is given in red, with the scale on the right. There are two striking features in

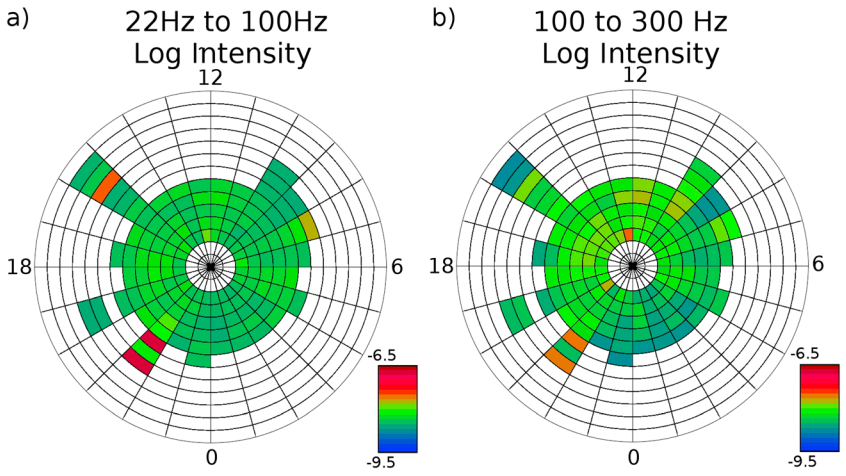

Figure 5. Plasmaspheric hiss intensity dependence on *L* and MLT. (a) The log of the wave intensity distribution for the ~22 Hz to 100 Hz band and (b) the log-intensity distribution for the ~100 Hz to the 300 Hz band.

this figure. The first and perhaps more interesting feature is that plasmaspheric hiss is present during positive *SYM-H* intervals. One can notice that plasmaspheric hiss has its highest occurrence rates for the range *SYM-H* = +15 nT to +75 nT. This will be addressed further later in this section.

The second feature is that plasmaspheric hiss is clearly present during intervals of negative *SYM-H* or during continuous substorms (HILDCAA intervals). There was no plasmaspheric hiss detected for *SYM-H* < -45 nT, but it is thought that this is an artifact due to the low number of storms during the interval of study and the spacecraft orbital constraints.

Prior *SYM-H* values of 1 h (brown), 2 h (green), and 3 h (blue) are also shown in the figure. This was included at the request of a referee. These latter delays show essentially the same results with each other. The only difference is that they do not include the extreme *SYM-H* events near +75 nT. The other histograms do, however, show the same small positive *SYM-H* dependences as in the zero lag data. Unfortunately, there are too few events to display a global view of these events. We will, however, show some detailed specific plasmaspheric hiss and hiss cases later in the paper.

3.3. Plasmaspheric Hiss Intensities

The plasmaspheric hiss average log intensities for different *L* and MLT are given in Figures 5 and 6 for different frequency ranges of the emission. Figure 5a gives the ~30 Hz to 100 Hz distribution, and Figure 5b the ~100 Hz to 300 Hz distribution. Figure 6a gives the ~300 Hz to 1 kHz distribution, and Figure 6b the ~1 kHz to 2 kHz distribution. The same color scale is used on all four panels of the two figures so that intercomparisons can be made among them. Thus, it can be noted that the lowest-frequency distribution, the plasmaspheric hiss component, is the most intense, and the highest-frequency component is the least intense.

The plasmaspheric hiss log intensities are relatively constant as a function of *L* and MLT. This is true for all four frequency ranges. One slight deviation from this general picture is that hiss is generally higher in some of the extended L shell events at the lowest-frequency ranges. Examples of this are the high-intensity (magenta) events at $L > 7$ in the dusk-premidnight sector of Figure 5a (~22 to 100 Hz).

A second noteworthy feature is that the waves have (~0.5 to 1 order of magnitude) greater intensities on the dayside in comparison to the nightside. This can be noted in Figures 5b and 6a for the ~100 Hz to 300 Hz (a difference of ~0.5 in log intensity) and ~300 Hz to 1 kHz (a difference of ~0.7 in log intensity). These two bands are the frequency range within which plasmaspheric hiss is typically detected.

The plasmaspheric hiss log-intensity distribution as a function of magnetic latitude is shown for all *L* inside the plasmasphere and all MLAT values in Figure 7. The vertical scale is in units of log intensity, and the statistical $\pm 1\sigma$ error bars are shown. The wave intensities are almost a constant 10^{-7} nT^2/Hz from the equator

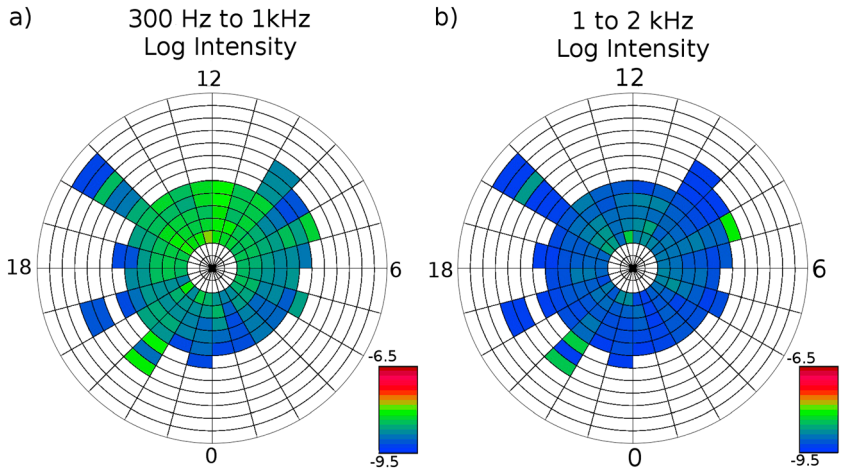

Figure 6. Same as in Figure 5 but for (a) ~300 Hz to 1 kHz and for (b) ~1 kHz to 2 kHz.

to ~55° (the 50° to 60° bin). There is a slight tendency for the emissions to be somewhat more intense near the equator. However, this difference is much below the 1σ level. The 50° to 60° MLAT range is the highest available due to spacecraft orbital constraints.

3.4. Plasmaspheric Hiss Waveforms and Coherency

A typical example of equatorial plasmaspheric hiss is shown in Figure 8 for a 5 April 1996 interval. The spacecraft was near local midnight (0044 MLT) and was in the equatorial plane (MLAT = −1.3°). The geomagnetic activity level was low (*AE* = 29 nT and *SYM-H* = −9 nT). The coordinates are in the minimum variance system for this particular ~0.4 s duration, where B1, B2, and B3 correspond to the wave magnetic field in the maximum, intermediate, and minimum variance directions. It can be noted that there are magnetic fluctuations in all three components, including the B3 component which is directed along the ambient magnetic field. Thus, there are fairly significant magnetic magnitude (compressional) components to the waves as well.

A smaller interval of Figure 8, 0.200 to 0.225 s, is shown in Figure 9. The three panels are the variation of the magnetic field magnitude, the B1 and B2 minimum variance components both in the middle panel, and the cross correlation between B1 and B2 at the bottom panel. It is noted that the cross correlation at −0.25 wavelength lag is ~0.5 whereas the value at +0.75 wavelength lag is ~0.2. The average cross correlation is thus ~0.35. Larger lags lead to even lower cross correlation coefficients. One would say that this wave interval is of general "low coherency." This is typical of plasmaspheric waves detected under ordinary conditions.

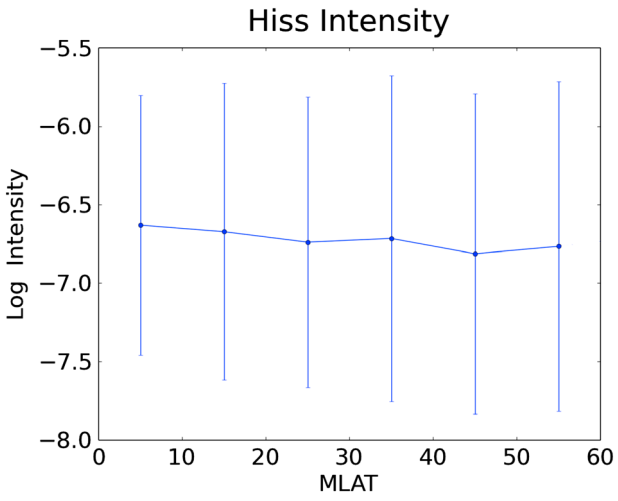

Figure 7. The plasmaspheric hiss intensity distribution as a function of MLAT for waves with frequencies between 22 and 100 Hz.

In the above figure there are many short intervals where there are several wave cycles that are adjacent to each other. One such interval is found near ~0.220 s. The insert of Figure 9 shows higher time resolution data for that interval. The coordinate system is the minimum variance for the shorter interval, and the format is the same as the main figure. It can be noted in Figure 9 (top) that there are variations in the magnetic field magnitude. The magnetic field deviations are largest when the wave amplitudes (Figure 9, middle) are also the largest. Examples can be found at ~0.204, 0.215, and 0.217 s. Obliquely propagating electromagnetic waves could cause such "compressional" effects.

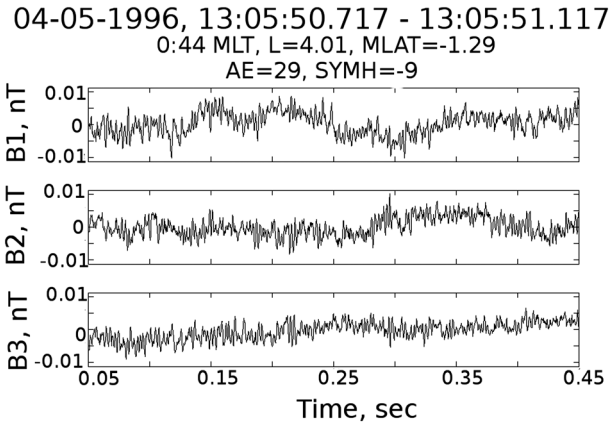

Figure 8. A typical example of equatorial plasmaspheric hiss. The waves were detected on 5 April 1996 at $L = 4$, at 0044 MLT, and MLAT = −1.3°.

Two individual wave cycles were examined in detail using the minimum variance technique for the specific intervals. The waves were found to be right-hand polarized, propagating slightly obliquely to the ambient magnetic field with $\theta_{kB0} = 29°$ and 37°, where θ_{kB0} is the angle between the wave **k** and the ambient magnetic field $\mathbf{B_0}$. The waves are slightly elliptically polarized. The values of λ_1/λ_2 and λ_2/λ_3 were 1.8 and 44.5 and 1.6 and 8.0 for the above two cases, respectively.

The insert of Figure 9 shows a different story however. This interval is focused on only ~2 wave cycles. The wave amplitudes are ~0.006 nT. What is notable about this smaller time interval of waves is that the wave coherency is quite high. The cross-correlation coefficient for −0.25 wavelength lag is 0.95, and the cross correlation for the +0.75 wavelength lag is 0.8, giving an average c.c. of ~0.9. So although the 0.200 to 0.225 s interval has overall low wave coherency, the shorter ~2 wavelength cycle from ~0.215 to 0.220 s has a high level of coherency. This latter feature is almost as high as chorus detected in the equatorial (generation) region [*Tsurutani et al.*, 2011a]. The values of λ_1/λ_2 and λ_2/λ_3 were 1.3 and 1.6 and 2.9 and 13.1 for above two cases, respectively.

The above plasmaspheric hiss interval was selected because it was typical of hiss detected in the plasmasphere. Plasmaspheric hiss is generally of low coherence (Figure 8) but with small pockets of high coherency as shown in the inset of Figure 9. This property of hiss was pointed out for modelers of wave-particle interactions.

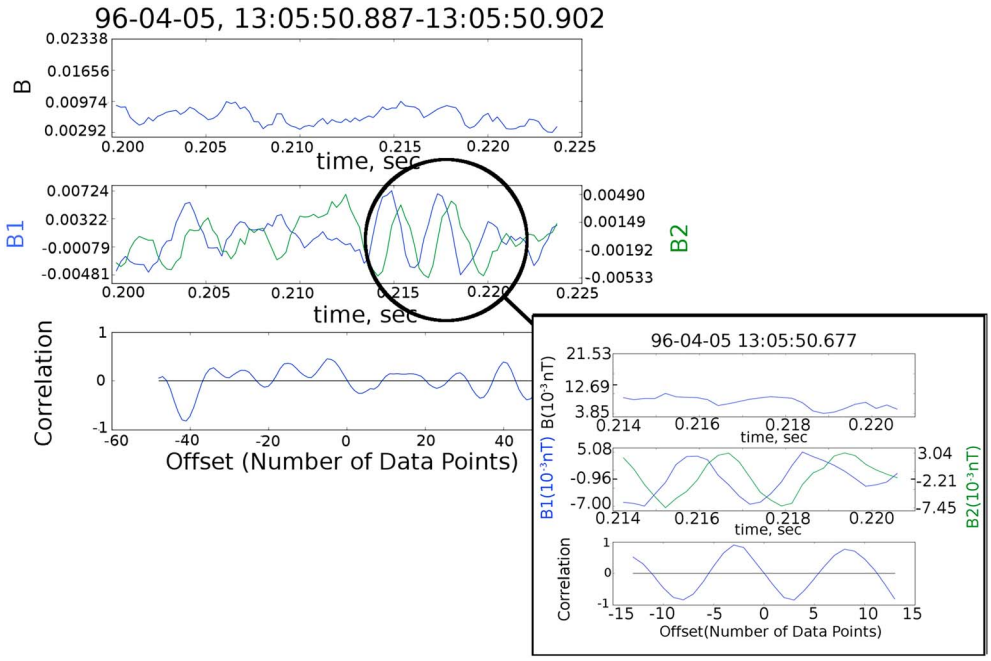

Figure 9. A ~0.022050 s section of Figure 8 in high time resolution. (top) The magnetic field magnitude perturbations. (middle) The B1 and B2 values. (bottom) The B1-B2 cross correlation as a function of lag. The insert (shown by a circle) is the same for a higher time resolution interval between ~0.215 and 0.220 s.

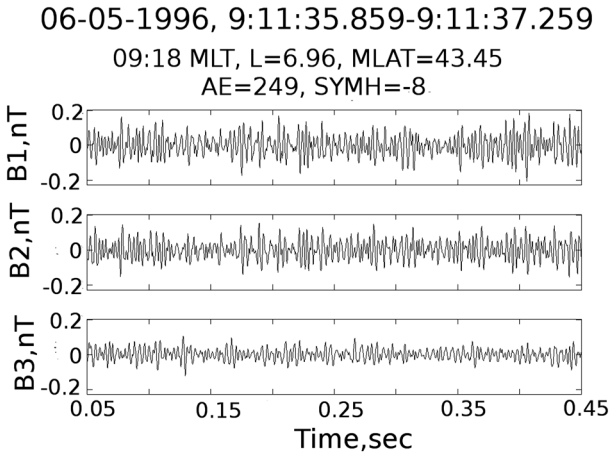

Figure 10. Hiss detected at $L = 7$. The same format as in Figure 8 is used.

3.5. Hiss at Large *L*

Figure 10 shows hiss detected on 5 June 1996 at $L = 7$. The event was detected at 0918 MLT at a MLAT of 43°. The geomagnetic activity at the time was moderate with $AE = 249$ nT and $SYM\text{-}H = -8$ nT. The characteristics of the hiss are different from the examples shown in Figures 8 and 9. The magnetic field components are shown in minimum variance coordinates. The waves have the largest amplitudes in the B1 and B2 components with B3 being the smallest. The B1 and B2 components are as large as ~±0.2 nT, considerably larger than those in Figures 8 and 9. The waves also appear far more coherent than those lower inside the plasmasphere. There are many consecutive wave cycles where B1 and B2 are correlated (not shown for brevity).

Figure 11 shows an example of hiss taken at $L = 8.9$, an even farther distance from the Earth than in Figure 10. The event occurred at a MLT = 0913 and a MLAT = 43° on 11 June 1996. The geomagnetic activity at the time was quiet, with $AE = 89$ nT and $SYM\text{-}H = 0$ nT. The wave characteristics of this event are similar to those of Figure 10: the waves that appear to be coherent are mainly transverse and have only small compressional components.

Figure 12 shows the wave coherency for an ~4 wave cycle interval from 0.220 to 0.240 s of Figure 11. The format is the same as in Figure 9. These waves are only slightly compressional with an ~0.010 nT component and with a ~0.025 nT peak-to peak transverse component. The peak correlation coefficient (Figure 12, bottom) is ~0.7 for the interval. These waves are coherent over many cycles. This is quite different from the character of waves detected deeper in the plasmasphere (Figures 8 and 9).

Minimum variance analyses were performed on individual wave cycles. A representative result is shown in Figure 13. The field in the B1, B2, and B3 directions is shown at the top. The B1-B2 hodogram is given in the bottom left panel, and the B1-B3 hodogram in the bottom right-hand panel. For the B1-B2 hodogram, the ambient magnetic field is into the paper. Thus, the polarization of the wave is right-hand elliptically polarized. The wave θ_{kB0} value is 73°. The degree of ellipticity, λ_1/λ_2, is ~2.0. The λ_2/λ_3 value was 13.1.

Three other wave cycles were examined. They too were right-hand elliptically polarized with highly obliquely directions of propagation ($\theta_{kB0} = 68°$, 69°, and 76°).

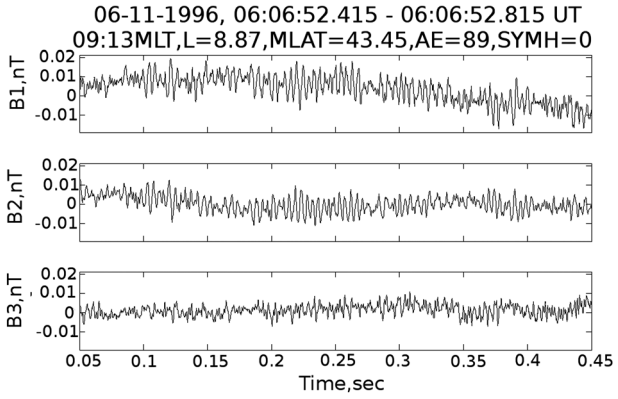

Figure 11. Hiss at $L = 8.9$. The format is the same as in Figure 8.

3.6. Plasmaspheric Hiss Inside the Plasmasphere During Intervals of High *SYM-H*

It was noted earlier that hiss occurred during geomagnetic quiet and also during intervals of high positive *SYM-H* values. The latter corresponds to intervals where the magnetosphere gets compressed by the high-solar wind ram pressure (see *Tsurutani et al.* [2011a] for a discussion of positive *SYM-H* intervals). This appears to be a case for a different hiss generation mechanism than was discussed in section 1. This topic will be discussed further in section 5.

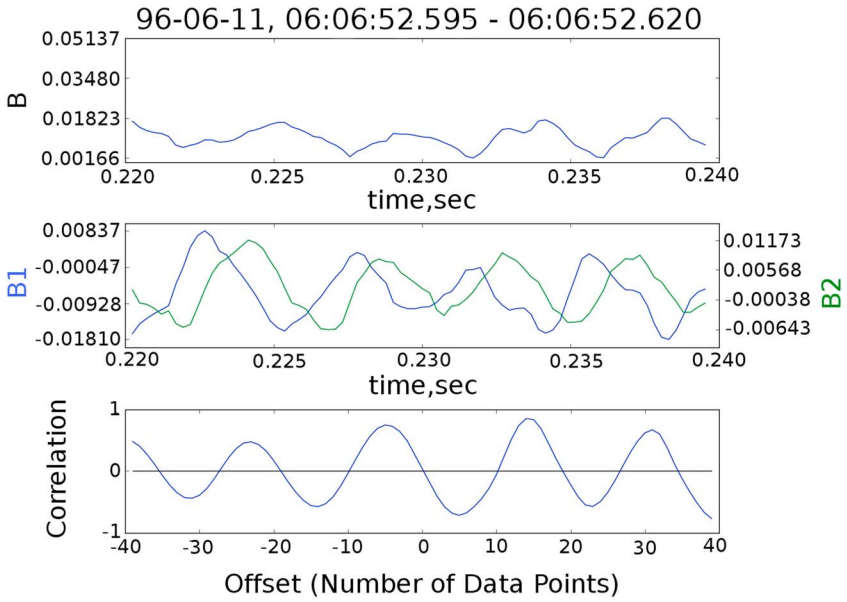

Figure 12. A small interval (0.220 to 0.240 s) from Figure 11. The format is the same as in Figure 9.

It is important to note what the characteristics of hiss are under these conditions. In Figure 14, we show a representative example of this type of hiss.

Figure 14 shows an example of hiss inside the plasmasphere on January 11, 1997 at 0145 UT. The Polar spacecraft was located on the dusk side at 1813 MLT and far off the equator at MLAT = −41°. *AE* was low, 137 nT, and the *SYM-H* was unusually high, +66 nT. The plasmaspheric hiss transverse amplitudes were ~ ±0.03 nT in the B1 component and ~± 0.02 nT in the B2 component. These values are considerably larger than that in Figures 8 and 9. This event is typical of a high-solar wind pressure event.

This plasmaspheric hiss is more coherent than what was shown in Figure 9 during nonhigh-pressure intervals. This is shown in more detail in Figure 15. This figure shows over 6 wave cycles. The format is the same as in Figure 9. The cross correlation for the B1 and B2 components is given in the third panel, and the value is ~0.8 for the interval for the range of −0.25 to +0.75 wavelengths. In this case the cross-correlation value decreases for ± 1 more wavelength and then increases again for ± 2 wavelengths. Thus, one notes that the wave train is coherent in general.

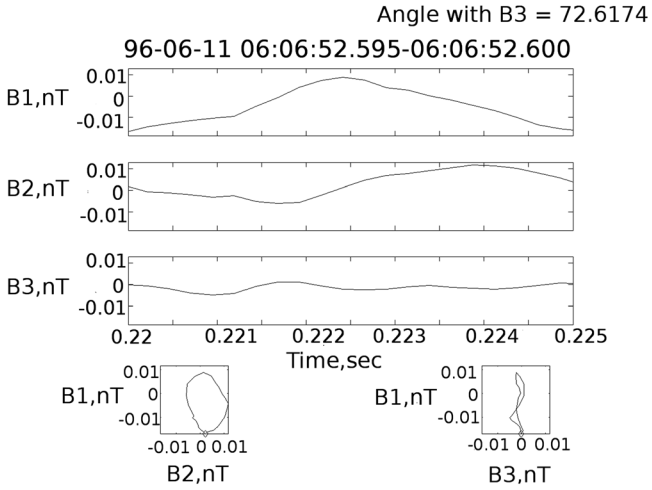

Figure 13. A wave cycle from Figure 12: 0.2200 to 0.2250 s. The wave is propagating at a 73° angle to the ambient magnetic field and has an ellipticity of ~2.0.

The properties of the individual wave cycles of Figure 15 were examine by the minimum variance method. The waves were found to be right-hand elliptically polarized, propagating obliquely to the ambient magnetic field. One example is shown in Figure 16.

The wave cycle in Figure 16 is representative of the waves in Figure 15. The θ_{kB0} for this event was 39°. The wave was elliptically polarized with $\lambda_1/\lambda_2 = 2.2$ and $\lambda_2/\lambda_3 = 3.9$. Several other cycles were examined in this interval. They were also elliptically polarized with angles of propagation of 31° and 37°.

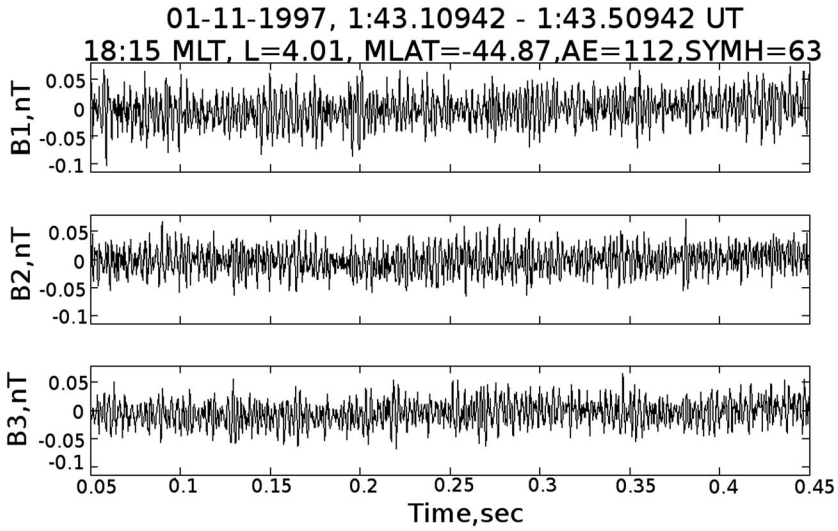

Figure 14. Plasmaspheric hiss inside the plasmasphere during high-solar wind pressure (*SYM-H* = +66 nT).

4. Summary

Analyses of a 1 year interval of Polar plasmaspheric hiss were performed. Magnetosonic and chorus waves were removed from the study by hand. The major plasmaspheric hiss findings were the following:

1. Electromagnetic whistler-mode plasmaspheric hiss was detected 32% of the time for all MLT and $L = 2$ to 7 during this study. Plasmaspheric hiss was detected at all magnetic local times, but occurred most frequently (51%) at dusk for the range $L = 3$ to 6 and 15 to 21 MLT. The source of these waves are most likely due to energetic (10–100 keV) electrons drifting into the plasmaspheric bulge region. The high thermal densities in the bulge lead to anisotropic electron instabilities, leading to local wave growth.
2. Plasmaspheric hiss was detected most frequently at the magnetic equator (38%). The occurrence frequency decreased with increasing magnetic latitude (Figure 2). Plasmaspheric hiss intensities in the

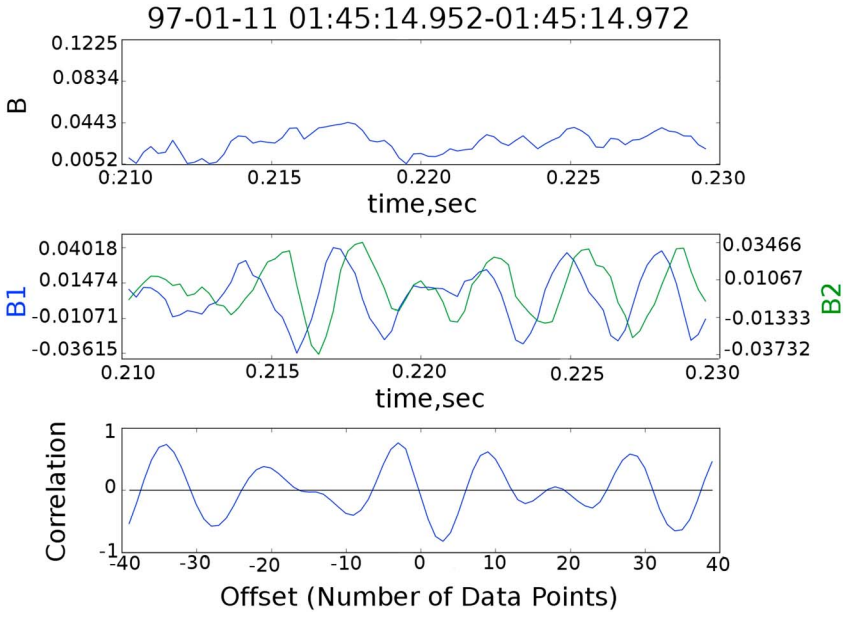

Figure 15. Wave coherency for 0.210 to 0.230 s of Figure 14. The format is the same as in Figure 9.

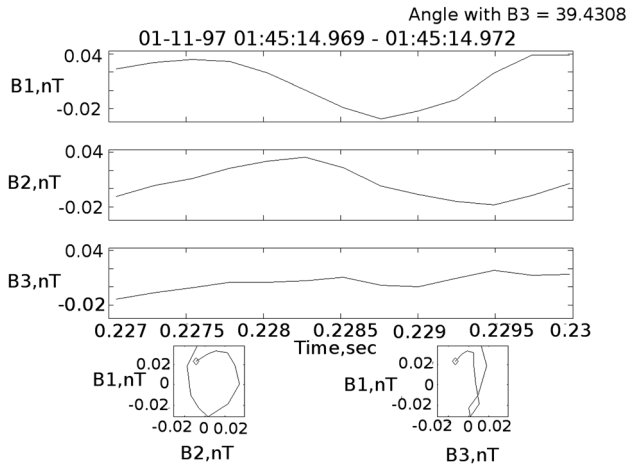

Figure 16. A wave cycle from Figure 15. The format is the same as in Figure 9.

frequency range of 22 Hz to 100 Hz have a constant average intensity of ~10^{-7} nT^2/Hz as a function of MLAT (Figure 7).

3. Plasmaspheric hiss in the frequency range from 22 Hz to 2 kHz has slightly higher intensities on the dayside (Figures 5 and 6), but other than that is nearly isotropic in *L* and MLT.
4. Plasmaspheric hiss was found to occur during both intervals of low *AE* and high *AE*. The majority of the waves were detected with $AE < 250$ nT or during geomagnetic quiet. Analyses assuming 30 min and 1 h delays in the plasmaspheric hiss from *AE* did not change this general picture.
5. One surprising new feature is that plasmaspheric hiss was frequently detected during high positive *SYM-H* values. This would correspond to high-solar wind ram pressure events (Figures 3 and 4). These plasmaspheric hiss emissions were more intense (up to ±0.03 nT) and had higher coherency properties during these intervals (Figures 14–16), even at large MLAT values. One obvious interpretation is that these are freshly created emissions which populate the plasmasphere. The *Lakhina et al*. [2010] wave-particle interaction model is appropriate here.
6. Plasmaspheric hiss under ordinary conditions is incoherent (Figure 8). Theoretical models which assume incoherent waves such as *Kennel and Petschek* [1966] are appropriate for modeling wave-particle interactions in these instances. However, there are small time intervals interspersed among the incoherent waves where the waves are quasi-coherent for a few cycles (Figure 9). For these cases, models involving coherent waves [*Lakhina et al*., 2010; *Bellan*, 2013] would be more appropriate.
7. When hiss was detected at large *L* values (up to 10), it occurred generally on the dusk-evening side (Figure 1). This hiss was large amplitude (up to 0.2 nT), quasi-coherent to coherent (Figures 10–13), and had higher intensities than those detected at lower *L*. Examples showing oblique propagation ($\theta_{kB0} = 70°$) and ellipticities of 2:1 were noted. Intense precipitation of energetic ~10–100 keV electrons may occur in the dusk local time sector due to these waves after substorm/storm electron injections at midnight, and the particles have drifted all the way through noon to the dusk region.

5. Discussion and Conclusions

We have performed a survey of plasmaspheric hiss for the purpose of understanding the wave properties in order to provide information for wave-particle modeling. We have obtained the basic numbers for wave intensities as functions of *L*, MLT, and MLAT.

Perhaps more importantly, we have also determined the wave coherency for different spatial locations and under different conditions. Plasmaspheric hiss under ordinary circumstances is almost incoherent with small patches of a few cycles of coherency. However, when solar wind density enhancements compress the magnetosphere, the wave intensities and coherency become considerably higher. Hiss detected at large *L* (>7) is generally more intense and coherent. This may be caused by energetic electrons drifting into plasma tails/plasmaspheric bulges and generating the hiss locally. This high coherency finding is in agreement with *Summers et al*. [2014] results, but during high-pressure intervals.

5.1. Plasmaspheric Hiss Day-Night Intensity Asymmetry

We first discuss past publications on plasmaspheric hiss properties during sudden impulse (SI^+)/interplanetary shocks because the topic is relevant to the interpretation of the plasmaspheric hiss day-night intensity asymmetry results found here. Plasmaspheric hiss intensifications have been noted during SI^+ events [*Gail and Inan*, 1990; *Shinbori et al*., 2003, and references therein]. SI^+s are mostly caused by interplanetary fast forward shock impingement onto the magnetosphere. The shocks cause a sudden (approximately seconds to minutes)

compression of the outer magnetosphere and the SI$^+$s at the ground [*Tsurutani et al*., 2008, 2014b]. *Kokubun* [1983] showed that the magnetospheric magnetic field was compressed only on the dayside (~0600 to ~1500 MLT) during SI$^+$ events. *Korth et al*. [1985] noted that both ELF-VLF wave amplitudes and electron pitch angle anisotropies increased if the spacecraft was on the dayside. *Gail and Inan* [1990] found that the waves were most enhanced in the region $3 < L < 6$, or in the plasmasphere, during SI$^+$ events. However, the latter authors found no LT or MLAT dependences in the waves.

Shinbori et al. [2003] has attempted to determine the source of the waves by studying 13 years of Akebono wave and energetic electron data during SI$^+$ events. They used the delay times between the SI$^+$ pulses and plasma wave and energetic electron changes to identify the signal propagation routes. They concluded that there were two propagation routes, one which "crosses the geomagnetic equatorial plane" and a second "which starts at the dayside cusp region and propagates from dayside to nightside through the polar ionosphere." They also note the triggering of auroral kilometric radiation (AKR) waves with some delay times. *Shinbori et al*. [2003] noted that there was no local time dependence of the plasma waves, similar to the results of *Gail and Inan* [1990].

In addition to the above SI$^+$ plasma wave studies, there have been UV auroral studies during SI$^+$ events as well. *Zhou and Tsurutani* [1999] and *Tsurutani et al*. [2001] have identified dayside auroras associated with shock impingement onto the magnetosphere. Their hypothesis was that the shocks compress preexisting dayside ~10–100 keV magnetospheric electrons, in agreement with the *Korth et al*. [1985] and *Kokubun* [1983] observations and conclusions [see also *Perona*, 1972]. *Zhou and Tsurutani* [1999] discussed only the compression of outer zone dayside ~10–100 keV remnant electrons and chorus generation. The chorus waves pitch angle scatters the electrons leading to precipitation into the ionosphere and the auroras that they observed. These chorus emissions could enter the plasmasphere by the *Bortnik et al*. [2009a, 2009b] mechanism. If the pressure increases associated with the shocks are particularly strong, energetic electrons drifting within the dayside plasmasphere could be compressed as well. These electrons could generate plasmaspheric hiss directly, but if the electron anisotropy is insufficient for direct instability, the wave circulation mechanism of *Thorne et al*. [1979] might be in operation.

The anisotropic ~10–100 keV dayside electrons will gradient and curvature drift from the dayside to the duskside plasmaspheric bulge. Electrons on relatively low L shells will drift into the plasmasphere and can generate plasmaspheric hiss directly.

Zhou and Tsurutani [2001] and *Tsurutani and Zhou* [2003] noted that the same shocks could trigger nighttime substorms as well. Since auroral kilometric radiation or AKR (detected during the previous cited SI$^+$ wave studies) are indications of substorms [*Calvert*, 2001], this indicates that substorm influences were present in the *Gail and Inan* [1990] and *Shinbori et al*. [2003] plasmaspheric hiss data sets as well. It is well known that substorms lead to plasma sheet energetic electron injections into the nightside magnetosphere [*Thorne et al*., 1973, 1974, 1977].

More recently, *Meredith et al*. [2004] have shown plasmaspheric hiss intensification dependence on substorms. Their hypothesis is that substorm convection electric fields will bring ~10–100 keV plasma sheet electrons into the plasmasphere, leading to local nightside plasmaspheric hiss generation. Gradient and curvature drift of electrons that are outside of the plasmasphere will cross the plasmasphere on the dayside leading to plasmaspheric hiss in that local time sector as well.

Thus, from the above discussion, there are at least three distinct local time regions of possible wave generation during SI$^+$/shock events, the dayside due to magnetospheric compression, the duskside due to electron gradient drift into the plasmaspheric bulge, and the nightside due to substorms. We need to consider all regions to better understand the plasmaspheric hiss MLT distributions found here. We also need to consider whether chorus is first generated in the outer magnetosphere and then propagates into the plasmasphere becoming plasmaspheric hiss [*Chum and Santolik*, 2005; *Bortnik et al*., 2008, 2009a; *Tsurutani et al*., 2012] or if the plasmaspheric hiss is generated directly inside the high density plasmasphere as proposed by *Thorne et al*. [1973] and *Meredith et al*. [2004].

As previously mentioned, there are very few interplanetary shocks or magnetic storms during this interval of study. That is because 1996–1997 was solar minimum. Thus, strong, impulsive, pressure pulses would not be expected to occur very often throughout this year of study nor would strong nightside inward convection, as occurs during magnetic storms. However, the solar wind is really never totally steady, especially in its

density variations. Thus, the physical principles will be the same. Small variations in the ram pressure may continuously generate chorus in the far outer zone minimum B pocket regions [*Tsurutani and Smith*, 1977; *Tsurutani et al*., 2009a]. The chorus generated there could find its way into the plasmasphere via the *Bortnik et al*. [2009a] propagation scenario. This would give the stronger plasmaspheric hiss dayside intensities as shown in this paper and in *Meredith et al*. [2004]. What could be a cause of these small pressure variations? It has been shown that interplanetary nonlinear Alfven waves phase steepen forming intermediate shocks and dissipate forming localized high density plasma regions through the ponderomotive force [*Tsurutani et al*., 2002a, 2002b, 2006, 2011c; *Dasgupta et al*., 2003]. These density variations can be a factor of ~2, causing sudden, but short duration, localized pressure variations on the magnetosphere. In this way, solar wind ram pressure fluctuations may be pumping free energy into the magnetosphere, ending up as plasmaspheric hiss waves.

It should be noted that this same argument cannot be used for the explanation of nightside plasmaspheric hiss being associated with chorus. Chorus generated in that local time sector during substorms is confined to ~10° MLAT [*Tsurutani and Smith*, 1974, 1977; *Tsurutani et al*., 2013; *Meredith et al*., 2001, 2012]. The waves are strongly Landau damped at higher MLATs and therefore cannot get to the high-latitude regions where they enter the plasmasphere (in the *Bortnik et al*. [2009a] scenario). Nightside plasmaspheric hiss must be generated directly by substorm energetic electrons [*Meredith et al*., 2004].

5.2. Intervals/Locations of High Wave Coherency

Plasmaspheric hiss has been found to be more intense and more coherent during high-solar wind pressure events. It should be noted that with coherent plasmaspheric hiss, modelers should consider the *Lakhina et al*. [2010], *Bellan* [2013], or other coherent wave theories to model wave-particle interactions.

The wave coherency for hiss detected outside of the plasmasphere ($L > 7$) is quite high. The wave amplitudes are high as well. These waves are most probably generated by energetic ~10–100 keV electron gradient drifting into plasma tails or extended plasmaspheric bulges. The higher plasma thermal densities lead to wave instability in these local regions. What is the source of these energetic electrons? They are most likely particles that are remnants of previous substorm or storm injections, as suggested by *Meredith et al*. [2004].

5.3. A Possible Plasmaspheric Hiss Scenario

We will try to summarize the sources of plasmaspheric hiss by three schematics given in Figure 17. Figure 17a shows the quiet time scenario, Figure 17b the high-solar wind pressure scenario, and Figure 17c the substorm/HILDCAA scenario. We do not show a magnetic storm model because of the lack of storm events during this survey.

Figure 17a shows a nominal plasmasphere and plasmaspheric hiss during quiet times (in black). Plasmaspheric hiss is generated in the duskside plasmaspheric bulge as remnant energetic electrons gradient drift into this region of space. Also shown in the figure (in color: Quiet + ΔT) is the recovery of the plasmasphere from continuous substorm (HILDCAA) activity. The plasmaspheric expansion causes remnant energetic electrons to be engulfed by the expanding plasmasphere, and hiss will be generated in the outer regions of the plasmasphere at all local times.

The color portion of Figure 17b shows chorus generated in the dayside outer magnetosphere during high-solar wind pressure events. This chorus propagates into the plasmasphere and becomes hiss. If the solar wind pressure is intense enough, energetic electrons within the plasmasphere may become unstable to hiss generation as well. Energetic electrons entering the plasmaspheric bulge region will generate hiss through the loss cone instability, as indicated in Figure 17a.

Figure 17c shows plasmaspheric hiss and chorus generation during sustained substorm (HILDCAA) intervals. Hiss will be generated in the nighttime sector by plasma sheet injection. As the outer zone energetic electrons gradient drift to dawn and local afternoon, they will generate chorus which may propagate into the plasmasphere and become hiss. Since sustained substorms will lead to convection electric fields which will convect the dayside plasmapause outward, energetic electrons will gradient drift into this region and generate hiss at these local times as well.

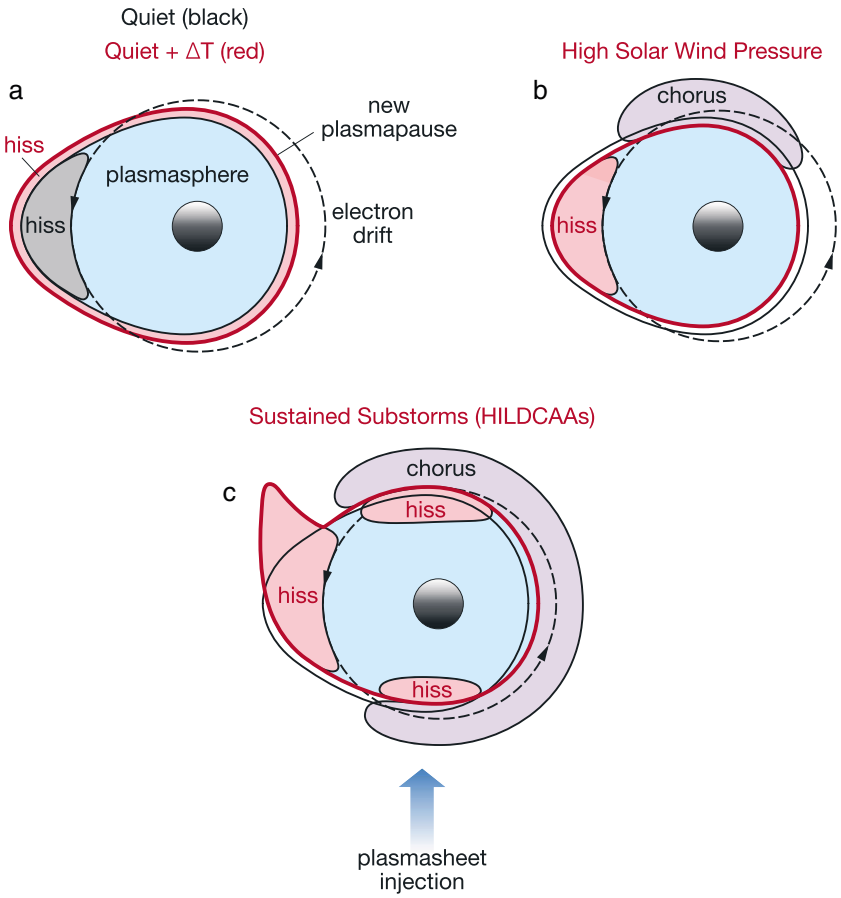

Figure 17. Plasmaspheric hiss generation regions during different solar wind and geomagnetic activity conditions: (a) during quiet (black plasmapause) and quiet time expansion (red plasmapause), (b) during high-solar wind pressure, and (c) during continuous substorms/HILDCAA intervals.

One topic which has not been discussed above is the possible conversion of magnetosonic waves into hiss though wave-particle interactions [*Tsurutani et al.*, 2013]. For this, we refer the reader to magnetosonic wave generation local time dependences [*Meredith et al.*, 2008; *Thorne*, 2010; *Tsurutani et al.*, 2013].

We note that some current works using GPS occultation data [*Verkhoglyadova et al.*, 2014] (A. J. Mannucci et al., Use of radio occultation to probe the high latitude ionosphere, submitted to *Atmospheric Measurement Techniques*, 2014) have identified enhanced ionization in the ~100–200 km altitude range at all local times during HILDCAA intervals. This is presumably due to energetic electron precipitation. This precipitation may be related to wave-particle interactions with enhanced plasmaspheric hiss. Further effort is needed to determine if this is correct or not.

6. Final Comments

Modeling of wave-particle interactions with hiss will depend on the location of the hiss and the solar wind and geomagnetic activity conditions at the particular time.

Hiss detected at large *L* has been shown to be coherent and large amplitude. Most of these events were noted to occur in the dusk-evening sector. It is assumed that these are freshly created waves at the location of detection. The wave-particle interactions should therefore be intense and the electron precipitation rate high. One would expect the bremsstrahlung X-rays detected at balloon altitudes to be broadband in energy, structureless, and have the overall profile of the electron cloud drifting through the plasma tail.

We reiterate that this was a survey done during solar minimum conditions when there was a lack of magnetic storms. The plasmaspheric hiss profile and properties might be considerably different under storm time conditions. We suggest that interested scientists conduct a survey of hiss properties under more geomagnetically active times as well.

Acknowledgments
We thank the two referees for their helpful comments and guide to sudden impulse papers that we were not aware of. Portions of this research were carried out at the Jet Propulsion Laboratory, California Institute of Technology under contract with NASA. Polar data can be obtained from NASA's Space Physics Data Facility. G.S.L. thanks the National Academy of Sciences of India for their support under the NASI Senior Scientist Platinum Jubilee Fellowship. O.S. acknowledges funding from GACR205-10.2279 and LH14010 grants.

Michael Balikhin thanks Atsuki Shinbori and another reviewer for their assistance in evaluating this paper.

References

Bellan, P. M. (2013), Pitch angle scattering of an energetic magnetic particle by a circularly polarized electromagnetic wave, *Phys. Plasmas*, *20*, 042117, doi:10.1063/1.4801055.

Bortnik, J., R. M. Thorne, and N. P. Meredith (2008), The unexpected origin of plasmaspheric hiss from discrete chorus emissions, *Nature*, *452*, 62–66, doi:10.1038/nature06741.

Bortnik, J., W. Li, R. M. Thorne, V. Angelopoulos, C. Cully, J. Bonnell, O. LeContel, and A. Roux (2009a), An observation linking the origin of plasmaspheric hiss to discrete chorus emissions, *Science*, *324*, 775–778.

Bortnik, J., R. M. Thorne, and N. P. Meredith (2009b), Plasmaspheric hiss overview and relation to chorus, *J. Atmos. Sol. Terr. Phys.*, *71*, 1636–1646.

Buchalet, L. J., and F. Lefeuvre (1981), One and two direction models for VLF electromagnetic waves observed on-board GEOS 1, *J. Geophys. Res.*, *86*, 2377–2383, doi:10.1029/JA086iA04p02377.

Calvert, W. (2001), Theory for the electron precipitation and current system that produces a magnetospheric substorm, *Phys. Plasmas*, *8*, 1099–1103.

Chan, K. W., and R. E. Holzer (1976), ELF hiss associated with plasma density enhancements in the outer magnetosphere, *J. Geophys. Res.*, *81*, 2267–2274, doi:10.1029/JA081i013p02267.

Chappell, C. R. (1974), Detached plasma regions in the magnetosphere, *J. Geophys. Res.*, *79*, 1861–1870, doi:10.1029/JA079i013p01861.

Chen, L., J. Bortnik, W. Li, R. M. Thorne, and R. B. Horne (2012), Modeling the properties of plasmaspheric hiss: 1. Dependence on chorus wave emission, *J. Geophys. Res.*, *117*, A05201, doi:10.1029/2011JA017201.

Chen, L., et al. (2014), Generation of unusually low frequency plasmaspheric hiss, *Geophys. Res. Lett.*, *41*, 5702–5709, doi:10.1002/2014GL060628.

Chum, J., and O. Santolik (2005), Propagation of whistler-mode chorus to low altitudes: Divergent ray trajectories and ground accessibility, *Ann. Geophys.*, *23*, 3727–3738.

Cornilleau-Wehrlin, N., R. Gendrin, F. Lefeuvre, M. Parrot, R. Grard, D. Jones, A. Bahnsen, E. Ungstrup, and W. Gibbons (1978), VLF electromagnetic waves observed onboard GEOS-1, *Space Sci. Rev.*, *22*, 371–382.

Cornilleau-Wehrlin, N., J. Solomon, A. Korth, and G. Kremser (1993), Generation mechanism of plasmaspheric ELF/VLF hiss: A statistical study from GEOS 1 data, *J. Geophys. Res.*, *98*, 21,471–21,480, doi:10.1029/93JA01919 .

Dasgupta, B., B. T. Tsurutani, and M. S. Janaki (2003), A kinetic approach to the ponderomotive force, *Geophys. Res. Lett.*, *30*(21), 2128, doi:10.1029/2003GL017385.

Delport, B., A. B. Collier, J. Lichtenberger, C. J. Rodger, M. Parrot, M. A. Clilverd, and R. H. W. Friedel (2012), Simultaneous observation of chorus and hiss near the plasmapause, *J. Geophys. Res.*, *117*, A12218, doi:10.1029/2012JA017609.

Dragonov, A. B., U. S. Inan, V. S. Sonwalkar, and T. F. Bell (1992), Magnetospherically reflected whistlers as a source of plasmaspheric hiss, *Geophys. Res. Lett.*, *19*, 233–236, doi:10.1029/91GL03167.

Dunckel, N., and R. A. Helliwell (1969), Whistler mode emissions on the OGO 1 satellite, *J. Geophys. Res.*, *74*, 6371–6385, doi:10.1029/JA074i026p06371.

Gail, W. B., and U. S. Inan (1990), Characteristics of wave-particle interactions during sudden commencements: 2. Spacecraft observations, *J. Geophys. Res.*, *95*(A1), 139–147, doi:10.1029/JA095iA01p00139.

Gail, W. B., U. S. Inan, R. A. Helliwell, D. L. Carpenter, S. Krisnaswamy, T. J. Rosenberg, and L. J. Lanzerotti (1989), Characteristics of wave-particle interactions during sudden commencements: 1. Ground-based observations, *J. Geophys. Res.*, *94*, 119–137, doi:10.1029/JA095iA01p00119.

Golden, D. I., M. Spasojevic, W. Li, and Y. Nishimura (2012), Statistical modeling of plasmaspheric hiss amplitude using solar wind measurements and geomagnetic indices, *Geophys. Res. Lett.*, *39*, L06103, doi:10.1029/2012GL051185.

Goldstein, B. E., and B. T. Tsurutani (1984), Wave normal directions of chorus near the equatorial source region, *J. Geophys. Res.*, *89*, 2789–2810, doi:10.1029/JA089iA05p02789.

Grebowsky, J. M. (1970), Model study of plasmapause motion, *J. Geophys. Res.*, *75*, 4329–4333, doi:10.1029/JA075i022p04329.

Green, J. L., S. Boardsen, L. Garcia, W. W. L. Taylor, S. F. Fung, and B. W. Reinisch (2005), On the origin of whistler mode radiation in the plasmasphere, *J. Geophys. Res.*, *110*, A03201, doi:10.1029/2004JA010495.

Gurnett, D. A., et al. (1995), The Polar plasma wave instrument, *Space Sci. Rev.*, *71*, 597–622, doi:10.1007/BF00751343.

Hajra, R., E. Echer, B. T. Tsurutani, and W. D. Gonzalez (2013), Solar cycle dependence of High-Intensity Long-Duration Continuous AE Activity (HILDCAA) events, relativistic electron predictors?, *J. Geophys. Res. Space Physics*, *118*, 5626–5638, doi:10.1002/jgra.50530.

Hayakawa, M., and S. S. Sazhin (1992), Mid-latitude and plasmaspheric HISS—A review, *Planet. Space Sci.*, *40*, 1325–1338, doi:10.1016/0032-0633(92)90089-7.

Hayakawa, M. Y., S. S. Tanaka, T. O. Sazhin, and K. Kurita (1986), Characteristics of dawnside mid-latitude VLF emissions associated with substorms as deduced from the two-stationed direction finding measurement, *Planet. Space Sci.*, *24*, 225–243.

Kennel, C. F., and H. E. Petschek (1966), Limit on stably trapped particle fluxes, *J. Geophys. Res.*, *71*, 1–28, doi:10.1029/JZ071i001p00001.

Kokubun, S. (1983), Characteristics of storm sudden commencement at geostationary orbit, *J. Geophys. Res.*, *88*, 10,025–10,033, doi:10.1029/JA088iA12p10025.

Korth, A., G. Kremser, N. Cornilleau-Wehrlin, and J. Solomon (1985), Observations of energetic electrons and VLF waves at geostationary orbit during storm sudden commencements (ssc), in *Solar Wind-Magnetospheric Coupling*, edited by J. Slavin and Y. Kamide, pp. 391–399, Am. Geophys. Univ. Press, Washington, D. C.

Lakhina, G. S., B. T. Tsurutani, O. P. Verkhoglyadova, and J. S. Pickett (2010), Pitch angle transport of electrons due to the cyclotron interactions with the coherent chorus subelements, *J. Geophys. Res.*, *115*, A00F15, doi:10.1029/2009JA014885.

Lefeuvre, F., M. Parrot, and C. Delannoy (1981), Wave distribution functions estimation of VLF electromagnetic waves observed onboard GEOS 1, *J. Geophys. Res.*, *86*, 2359–2375, doi:10.1029/JA086iA04p02359.

Li, W., et al. (2013), An unusual enhancement of low-frequency plasmaspheric hiss in the outer plasmasphere associated with substorm-injected electrons, *Geophys. Res. Lett.*, *40*, 3798–3803, doi:10.1002/grl.50787.

Meredith, N. P., R. B. Horne, and R. R. Anderson (2001), Substorm dependence of chorus amplitudes: Implications for the acceleration of electrons to relativistic energies, *J. Geophys. Res.*, *106*, 13,165–13,178, doi:10.1029/2000JA900156.

Meredith, N. P., R. B. Horne, R. M. Thorne, D. Summers, and R. R. Anderson (2004), Substorm dependence of plasmaspheric hiss, *J. Geophys. Res.*, *109*, A06209, doi:10.1029/2004JA010387.
Meredith, N. P., R. B. Horne, M. A. Clilverd, D. Horsfall, R. M. Thorne, and R. R. Anderson (2006), Origins of plasmaspheric hiss, *J. Geophys. Res.*, *111*, A09217, doi:10.1029/2006JA011707.
Meredith, N. P., R. B. Horne, and R. R. Anderson (2008), Survey of magnetosonic waves and proton ring distributions in the Earth's inner magnetosphere, *J. Geophys. Res.*, *113*, A06213, doi:10.1029/2007JA012975.
Meredith, N. P., R. B. Horne, A. Sicard-Piet, D. Boscher, H. Yearby, W. Li, and R. M. Thorne (2012), Global model of lower band and upper band chorus from multiple satellite observations, *J. Geophys. Res.*, *117*, A10225, doi:10.1029/2012JA017978.
Parrot, M., and F. Lefeuvre (1986), Statistical study of the propagation characteristics of ELF hiss observed on GEOS-1, inside and outside the plasmasphere, *Ann. Geophys.*, *4*, 363–383.
Perona, G. E. (1972), Theory on the precipitation of magnetospheric electrons at the time of a sudden commencement, *J. Geophys. Res.*, *77*, 101–111, doi:10.1029/JA077i001p00101.
Russell, C. T., R. E. Holzer, and E. J. Smith (1969), OGO 3 Observations of ELF noise in the magnetosphere: 1. Spatial extent and frequency of occurrence, *J. Geophys. Res.*, *74*, 755–777, doi:10.1029/JA074i003p00755.
Santolik, O., and J. Chum (2009), The origin of plasmaspheric hiss, *Science*, *324*(5928), 729–730, doi:10.1126/science.1172878.
Santolik, O., M. Parrot, L. R. O. Storey, J. S. Pickett, and D. A. Gurnett (2001), Propagation analysis of plasmaspheric hiss using Polar PWI measurements, *Geophys. Res. Lett.*, *28*, 1127–1130, doi:10.1029/2000GL012239.
Santolik, O., J. Chum, M. Parrot, D. A. Gurnett, J. S. Pickett, and N. Cornilleau-Wehrlin (2006), Propagation of whistler mode chorus to low altitudes: Spacecraft observations of structured ELF hiss, *J. Geophys. Res.*, *111*, A10208, doi:10.1029/2005JA011462.
Shinbori, A., T. Ono, M. Iizima, and A. Kumamoto (2003), Sudden commencements related plasma waves observed by the Akebono satellite in the polar region and inside the plasmasphere region, *J. Geophys. Res.*, *108*(A12), 1457, doi:10.1029/2003JA009964.
Smith, E. J., and B. T. Tsurutani (1976), Magnetosheath lion roars, *J. Geophys. Res.*, *81*, 2261–2266, doi:10.1029/JA081i013p02261.
Smith, E. J., A. M. A. Frandsen, B. T. Tsurutani, R. M. Thorne, and K. W. Chan (1974), Plasmaspheric hiss intensity variations during magnetic storms, *J. Geophys. Res.*, *79*, 2507–2510, doi:10.1029/JA079i016p02507.
Solomon, J., N. Cornilleau-Wehrlin, A. Korth, and G. Kremser (1988), An experimental study of ELF/VLF hiss generation in the Earth's magnetosphere, *J. Geophys. Res.*, *93*, 1839–1847, doi:10.1029/JA093iA03p01839.
Storey, L. R. O., and F. Lefeuvre (1979), The analysis of 6-component measurements of a random electromagnetic wave field in a magnetoplasma—I. The direct problem, *Geophys. J. R. Astron. Soc.*, *56*, 255–269.
Storey, L. R. O., F. Lefeuvre, M. Parrot, L. Cairo, and R. R. Anderson (1991), Initial survey of the wave distribution functions for plasmaspheric hiss observed by ISEE 1, *J. Geophys. Res.*, *96*(A11), 19,469–19,489, doi:10.1029/91JA01828.
Summers, D., Y. Omura, S. Nakamura, and C. A. Kletzing (2014), Fine structure of plasmaspheric hiss, *J. Geophys. Res. Space Physics*, *119*, 9134–9149, doi:10.1002/2014JA020437.
Thorne, R. M. (2010), Radiation belt dynamics: The importance of wave-particle interactions, *Geophys. Res. Lett*, *37*, L22107, doi:10.1029/2010GL044990.
Thorne, R. M., E. J. Smith, R. K. Burton, and R. E. Holzer (1973), Plasmaspheric hiss, *J. Geophys. Res.*, *78*, 1581–1596, doi:10.1029/JA078i010p01581.
Thorne, R. M., E. J. Smith, K. J. Fiske, and S. R. Church (1974), Intensity variation of ELF hiss and chorus during isolated substorms, *Geophys. Res. Lett.*, *1*, 193–196, doi:10.1029/GL001i005p00193.
Thorne, R. M., S. R. Church, W. J. Malloy, and B. T. Tsurutani (1977), The local time variation of ELF emissions during periods of substorm activity, *J. Geophys. Res.*, *82*, 1585–1590, doi:10.1029/JA082i010p01585.
Thorne, R. M., S. R. Church, and D. J. Gorney (1979), On the origin of plasmaspheric hiss: The importance of wave propagation and the plasmapause, *J. Geophys. Res.*, *84*, 5241–5247, doi:10.1029/JA084iA09p05241.
Tsurutani, B. T., and W. D. Gonzalez (1987), The cause of high-intensity long-duration continuous AE activity (HILDCAAS): Interplanetary Alfven wave trains, *Planet. Space Sci.*, *35*(4), 405–412.
Tsurutani, B. T., and E. J. Smith (1974), Postmidnight chorus: A substorm phenomenon, *J. Geophys. Res.*, *79*, 118–127, doi:10.1029/JA079i001p00118.
Tsurutani, B. T., and E. J. Smith (1977), Two types of magnetospheric ELF chorus and their substorm dependences, *J. Geophys. Res.*, *82*(32), 5112–5128, doi:10.1029/JA082i032p05112.
Tsurutani, B. T., and X.-Y. Zhou (2003), Interplanetary shock triggering of substorms: WIND and POLAR, *Adv. Space Res.*, *31*, 1063–1067.
Tsurutani, B. T., E. J. Smith, and R. M. Thorne (1975), Electromagnetic hiss and relativistic electron losses in the inner zone, *J. Geophys. Res.*, *80*, 600–607, doi:10.1029/JA080i004p00600.
Tsurutani, B. T., X.-Y. Zhou, V. M. Vasyliunas, G. Haerendel, J. K. Arballo, and G. S. Lakhina (2001), Interplanetary shocks, magnetopause boundary layers and dayside auroras: The importance of a very small magnetospheric region, *Surv. Geophys.*, *22*, 101–130.
Tsurutani, B. T., C. Galvan, J. K. Arballo, D. Winterhalter, R. Sakurai, E. J. Smith, B. Buti, G. S. Lakhina, and A. Balogh (2002a), Relationship between discontinuities, magnetic holes, magnetic decreases, and nonlinear Alfven waves: Ulysses observations over the solar poles, *Geophys. Res. Lett.*, *29*(11), 1528, doi:10.1029/2001GL013623.
Tsurutani, B. T., B. Dasgupta, C. Galvan, M. Neugebauer, G. S. Lakhina, J. K. Arballo, D. Winterhalter, B. E. Goldstein, and B. Buti (2002b), Phase-steepened Alfven waves, proton perpendicular energization and the creation of magnetic holes and magnetic decreases: The ponderomotive force, *Geophys. Res. Lett.*, *29*(24), 2233, doi:10.1029/2002GL015652.
Tsurutani, B. T., et al. (2006), Corotating solar wind streams and recurrent geomagnetic activity: A review, *J. Geophys. Res.*, *111*, A07S01, doi:10.1029/2005JA011273.
Tsurutani, B. T., E. Echer, F. L. Guarnieri, and J. U. Kozyra (2008), CAWSES November 7–8, superstorm: Complex solar and interplanetary features in the post-solar maximum phase, *Geophys. Res. Lett.*, *35*, L06S05, doi:10.1029/2007GL031473.
Tsurutani, B. T., O. P. Verkhoglyadova, G. S. Lakhina, and S. Yagitani (2009), Properties of dayside outer zone chorus during HILDCAA events, Loss of energetic electrons, *J. Geophys. Res.*, *114*, A03207, doi:10.1029/2008JA013353.
Tsurutani, B. T., B. J. Falkowski, O. P. Verkhoglyadova, J. S. Pickett, O. Santolik, and G. S. Lakhina (2011a), Quasi-coherent chorus properties: 1. Implications for wave-particle interactions, *J. Geophys. Res.*, *116*, A09210, doi:10.1029/2010JA016237.
Tsurutani, B. T., E. Echer, and W. D. Gonzalez (2011b), The solar and interplanetary causes of the recent minimum in geomagnetic activity (MGA23): A combination of midlatitude small coronal holes, low IMF Bz variances, low solar wind speeds and low solar magnetic fields, *Ann. Geophys.*, *29*, 1–17, doi:10.5194/angeo-29-1-2011.
Tsurutani, B. T., G. S. Lakhina, O. P. Verkhoglyadova, E. Echer, F. L. Guarnieri, Y. Narita, and D. O. Constantinescu (2011c), Magnetosheath and heliosheath mirror mode structures, interplanetary magnetic decreases, and linear magnetic decreases: Differences and distinguishing features, *J. Geophys. Res.*, *116*, A02103, doi:10.1029/2010JA015913.

Tsurutani, B. T., B. J. Falkowski, O. P. Verkhoglyadova, J. S. Pickett, O. Santolik, and G. S. Lakhina (2012), Dayside ELF electromagnetic wave survey: A Polar statistical study of chorus and hiss, *J. Geophys. Res.*, *117*, A00L12, doi:10.1029/2011JA017180.

Tsurutani, B. T., G. S. Lakhina, and O. P. Verkhoglyadova (2013), Energetic electron (>10 keV) microburst precipitation, ~5-15s x-ray pulsations, chorus and wave-particle interactions: A review, *J. Geophys. Res. Space Physics*, *118*, 2296–2312, doi:10.1002/jgra.50264.

Tsurutani, B. T., B. J. Falkowski, J. S. Pickett, O. P. Verkhoglyadova, O. Santolik, and G. S. Lakhina (2014a), Extremely intense ELF magnetosonic waves: A survey of Polar observations, *J. Geophys. Res. Space Physics*, *119*, 964–977, doi:10.1002/2013JA019284.

Tsurutani, B. T., E. Echer, K. Shibata, O. P. Verkhoglyadova, A. J. Mannucci, W. D. Gonzalez, J. U. Kozyra, and M. Pätzold (2014b), The interplanetary causes of geomagnetic activity during the 7–17 March 2012 interval: A CAWSES II overview, *J. Space Weather Space Clim.*, *4*, A02, doi:10.1051/swsc/2013056.

Verkhoglyadova, O. P., B. T. Tsurutani, and G. S. Lakhina (2010), Properties of obliquely propagating chorus, *J. Geophys. Res.*, *115*, A00F19, doi:10.1029/2009JA014809.

Verkhoglyadova, O. P., A. J. Mannucci, B. T. Tsurutani, M. G. Mlynczak, L. A. Hunt, R. J. Redmon, and J. C. Green (2014), Localized thermosphere ionization events during the high speed stream interval of 29 April–5 May 2011, *J. Geophys. Res. Space Physics*, doi:10.1002/2014JA020535.

Wang, C., Q. Zong, F. Xiao, Z. Su, Y. Wang, and C. Yue (2011), The relations between magnetospheric chorus and hiss inside and outside the plasmasphere boundary layer: Cluster observation, *J. Geophys. Res.*, *116*, A07221, doi:10.1029/2010JA016240.

Zhou, X.-Y., and B. T. Tsurutani (1999), Rapid intensification and propagation of the dayside aurora: Large scale interplanetary pressure pulses (fast shocks), *Geophys. Res. Lett.*, *26*, 1097–1100, doi:10.1029/1999GL900173.

Zhou, X.-Y., and B. T. Tsurutani (2001), Interplanetary shock triggering of nightside geomagnetic activity: Substorms, pseudobreakups, and quiescent events, *J. Geophys. Res.*, *106*, 18,957–18,967, doi:10.1029/2000JA003028.